Accepted Manuscript

Covariability of seasonal temperature and precipitation over the Iberian Peninsula in high-resolution regional climate simulations (1001–2099)

S. Fernández-Montes, J.J. Gómez-Navarro, F.S. Rodrigo, J.A. García-Valero, J.P. Montávez

Please cite this article as: Fernández-Montes, S., Gómez-Navarro, J.J., Rodrigo, F.S., García-Valero, J.A., Montávez, J.P., Covariability of seasonal temperature and precipitation over the Iberian Peninsula in high-resolution regional climate simulations (1001–2099), *Global and Planetary Change* (2016), doi: 10.1016/j.gloplacha.2016.09.007

Covariability of seasonal temperature and precipitation over the Iberian Peninsula in high-resolution regional climate simulations (1001-2099)

S.Fernández-Montes[12]*, J.J. Gómez-Navarro[13], F.S.Rodrigo[2], J.A. García-Valero[14], J.P.Montávez[1]

1. Department of Physics, University of Murcia, Spain
2. Department of Chemistry and Physics, University of Almería, Spain
3. Physics Institute, University of Bern, Switzerland
4. Spanish Meteorology Institute (AEMET). Murcia, Spain

*Corresponding author: Sonia Fernández Montes. Department of Chemistry and Physics – University of Almeria, Carretera de Sacramento s/n. La Cañada de San Urbano, 04120, Almeria, Spain. email: soniafm@ual.es

Abstract

Precipitation and surface temperature are interdependent variables, both as a response to atmospheric dynamics and due to intrinsic thermodynamic relationships and feedbacks between them. This study analyzes the covariability of seasonal temperature (T) and precipitation (P) across the Iberian Peninsula (IP) using regional climate paleosimulations for the period 1001-1990, driven by reconstructions of external forcings. Future climate (1990-2099) was simulated according to SRES scenarios A2 and B2. These simulations enable exploring, at high spatial resolution, robust and physically consistent relationships.

In winter, positive P-T correlations dominate west-central IP (Pearson correlation coefficient ρ = +0.43, for 1001-1990), due to prevalent cold-dry and warm-wet conditions, while this relationship weakens and become negative towards mountainous, northern and eastern regions. In autumn, negative correlations appear in similar regions as in winter, whereas for summer they extend also to the N/NW of the IP. In spring, the whole IP depicts significant negative correlations, strongest for eastern regions (ρ = -0.51). This is due to prevalent frequency of warm-dry and cold-wet modes in these regions and seasons. At the temporal scale, regional correlation series between seasonal anomalies of temperature and precipitation (assessed in 31 years running windows in 1001-1990) show very large multidecadal variability. For winter and spring, periodicities of about 50-60 years arise. The frequency of warm-dry and cold-wet modes appears correlated with the North Atlantic Oscillation (NAO), explaining mainly co-variability changes in spring. For winter and some regions in autumn, maximum and minimum P-T correlations appear in periods with enhanced meridional or easterly circulation (low or high pressure anomalies in the Mediterranean and Europe). In spring and summer, the Atlantic Multidecadal Oscillation shows some fingerprint on the frequency of warm/cold modes.

For future scenarios, an intensification of the negative P-T relationship is generally found, as a result of an increased frequency of the warm-dry mode.

Keywords: Iberian Peninsula, Precipitation-temperature covariability, Mediterranean climate, Multidecadal variability, seasonal changes

Highlights:

Regional simulations for the Iberian Peninsula are employed (1001-2099). Precipitation-temperature relationship is studied. Positive correlations dominate west-central region in winter. Negative correlations arise in mountainous regions in all seasons. In spring, all regions depict negative correlations, enhanced in warmer periods.

1. Introduction

In climate studies, the joint analysis of precipitation and temperature variability provides insight into the behaviour of heat and moisture modes which are usually more relevant for environmental, agricultural and societal impacts (López-Moreno et al. 2011; Estrella and Menzel 2013) than the study of anomalies in one variable independently.

Precipitation-temperature interrelationship depends on the climatic regime, time of the year and temporal scale considered. Changes in the hydrological cycle and precipitation are coming along with changes in temperature (Trenberth 2011). The water vapor holding capacity of the lower troposphere increases by ~7% per degree of temperature (following the Clausius-Clapeyron relationship), this vapor acts in turn as a positive-feedback (greenhouse gas) towards warming. However, observed and simulated changes in precipitation do not follow such saturation water vapor rate with temperature, principally due to energetic constraints of evaporation (limited by moisture availability) and condensation processes (Li et al. 2013).

In winter at mid and high latitudes, daily precipitation intensity shows a general increase with temperature (as shown for most Europe, Berg et al. 2009), since moisture is available from oceans and precipitation is mainly related to warm-moist advection in extratropical cyclones, favoring a warm-wet mode. However, normal low winter temperatures set a limit in the water-holding capacity of the atmosphere (saturation is reach soon under cold conditions, limiting the amount of precipitation), hence the combination dry-cold is also frequent. In consequence, a positive

temperature-precipitation correlation is found for winter months at high latitudes (Trenberth and Shea 2006; Adler et al. 2008), above 40º latitude. Conversely, in summer the availability of moisture, and not the atmosphere's capacity to hold this moisture, is the dominant factor for limiting precipitation intensity (Berg et al. 2009). An important precipitation-to-temperature causal relationship is expected in summer, as dry conditions relates with more sunshine and less evaporative cooling, while wet summers are cool (moisture acts as a "air conditioner" and, moreover, clouds blocks the input radiation), explaining the observed negative P-T correlations over land in the warm season (Trenberth and Shea 2005; Déry and Wood 2005; Adler et al. 2008, Wu et al. 2013; Berg et al. 2015). Seasonal dependence is more obvious over land than over ocean and is strongest over the mid- and high-latitudes than over the tropics (Wu et al. 2013). Over tropical and subtropical oceans, it is well known that higher Sea Surface Temperature (SST) anomalies are accompanied by increased convection and rainfall (like in El Niño phenomenon) (Trenberth and Shea 2005).

A key ingredient in the correlations between precipitation and temperature is the magnitude of the variability. In this respect, considering the global scale, precipitation variability is higher in the tropics than at high latitudes, while the reverse is true for temperature (Adler et al. 2008). In tropical regions, El Niño-Southern Oscillation (ENSO) is found to be a dominant factor in the interannual precipitation-temperature relations, while both ENSO and Artic Oscillation (AO) seem to modulate this relationship north of the equator (Adler et al. 2008). A strong seasonal change in the P-T relation tends to occur in the Northern Hemisphere higher latitudes (positive relationship in winter, negative in summer). Thus the linear correlations between these two variables indicate both regional interactions between precipitation and surface temperature, and the remote modulations of large-scale circulation anomalies (Adler et al. 2008). Less works have investigated P-T covariability on regional scales, where land-atmosphere (and also ocean-land) interactions and orography should play an important role. For Europe, a few studies considering seasonal precipitation-temperature co-variability are found, only for the British Islands (Tout 1987) and Switzerland (Rebetez 1996). Rodrigo 2014 explored P-T covariability using four station series in the IP, but no literature with regional focus at high-resolution is found for the IP. Thus, recent published works about P-T relationship consider global datasets and models with low spatial resolution. Moreover, they focussed only on winter and summer extended seasons (Adler et al., 2008; Trenberth and Shea 2005; Wu et al. 2013; Berg et al. 2015). In the IP, inter-seasonal climate variability is very important, being as well precipitation and temperature anomalies in the transition seasons relevant for the annual water balance (De Luis et al. 2010) and for other environmental/societal issues.

From global to regional scales, it is crucial to get reliable estimations of the amplitude of natural variability on multidecadal and longer temporal scales, in order to improve the attribution of climate

change to natural and anthropogenic forcing (e.g. Schurer et al. 2013). However, complete and reliable long-term observations are scarce (and mostly limited to last century), and proxy-based reconstructions (tree rings, etc) provide valuable but local climatic information (e.g., Amann et al. 2015). Despite its large computational cost, the added value of a Regional Climate Model (RCM) such as MM5 is that it is able to simulate a reliable, physically consistent climate that takes into account the characteristics due to high resolution orographic features, such as over the Iberian Peninsula (Jerez et al. 2010; Gómez-Navarro et al. 2011). Therefore, even if simulated variability is not temporally coherent with real past climate -due to the high level of internal variability and the lack of data assimilation (Gómez-Navarro et al. 2012)-, it allows to explore the physical relationships between T and P over a long period (under a large range of different climatic conditions), improving reliability on the estimations. Previous works about P-T relationship analyze rather short periods of a few decades (Trenberth and Shea 2005, Adler at al., 2008). For last decades, comparison of results in the P-T relationship from observations and regional models show a good agreement both on a daily (Berg et al. 2009), monthly (Trenberth and Shea 2005) and annual timescales (Adler et al. 2008), manifiesting the capability of models to realistically simulate the physical links between both variables.

In a previous work, Gómez-Navarro et al. (2012) explore the role of internal variability and external forcings on temperature and precipitation over the IP, by means of two regional paleosimulations (differing just on their initial conditions) over the period 1001-1990 CE, focusing only in winter and summer. They found that temperature responds homogeneously to the external factors at most temporal scales, whereas precipitation is more governed by internal variability. However, precipitation in mountainous regions in winter, as well as summer precipitation towards N/NW IP was found to be some related to external forcings (checked by comparing precipitation in both simulations). In the cited work, P-T correlations were checked on the low frequency (after applying 31 years running means to the variables). In winter, considering this low-pass filter, significant negative correlations appeared in mountainous regions, found related with an increase/decrease in the cloud condensation level with increasing/decreasing temperature (Lawrence 2005). Significant positive correlations in winter were found only over a very small region in the SW IP. In summer, P-T negative correlations were obtained over the North and W/NW (Gómez-Navarro et al. 2012).

In this work, we aim to extend that study to the analysis of P-T relationships with special focus on interannual timescales, which were not previously explored using these above mentioned simulations. Moreover, we aim to analyze for all seasons temporal changes in the P-T relationship (on decadal to longer time scales) and associated physical mechanisms, with focus also on the transitional seasons. Therefore, we aim to explore here for first time in the IP the covariability between seasonal P and T in a comprehensive and physical- robust analysis based on the thousand years of simulated data by Gómez-Navarro et al. (2011), Gómez-Navarro et al. (2012).

Changes in the P-T covariability in future Special Report on Emissions Scenarios (SRES) A2 and B2 (Gómez-Navarro et al. 2010) are also investigated.

2. Data and methods

This study employs two simulations carried out with a climate version of the Mesoscale Model MM5 driven by the global model ECHO-G. This model configuration has been profusely described and its skill critically assessed in previous studies, so the reader is referred to the original publications for further details (Gómez-Navarro et al. 2011; 2012; 2013). The forcings used to drive both simulations include changes in the Total Solar Irradiance (TSI), greenhouse gas concentrations and volcanic activity. The latter is taken into account through an effective reduction in the TSI. The way these forcings are introduced and their evolution is the same as in the GCM for the sake of consistency.

The simulations, hereafter referred as MM5-ERIK1 and MM5-ERIK2, span the past millennium almost entirely (1001-1990). Both simulations are the result of nesting the MM5 model to the respective simulations ERIK1 and ERIK2, carried out with the ECHO-G model, and differ only in the initial condition used to initiate the latter (ERIK1 starts with warmer climate). The domains for MM5 consist of two two-way nested domains (See Figure 1 in Gómez-Navarro et al. 2011), with an inner domain implementing a resolution of 30 km over the IP. The ECHO-G model driving the regional simulations consists of the spectral atmospheric model ECHAM4 (used with a horizontal resolution $3.75° \times 3.75°$) coupled to the ocean model HOPE-G. These domains, as well as the chosen physical parametrization, are the same as those previously described by Gómez-Navarro et al. (2011; 2012).

The external forcings considered are: Greenhouse gases (GHGs), total solar irradiance (TSI) and Global mean radiative forcing of volcanic aerosol, all of them provided by Crowley (2000) (Supplementary material, Fig. S1). The ocean, and in particular the Sea surface temperature, is not simulated by MM5, but taken from the driving global model and considered as a time-varying boundary condition. This implies that there are no explicit feedbacks between the atmosphere and the ocean within the regional domains. Only the feedbacks simulated within the GCM are indirectly considered, since they are introduced through the boundaries of the mother domain. Further, the changes in the external factors do not include changes in land use and a dynamic response of vegetation to climate change. These limitations are due to the lack of reliable information and model advances available at the time of the execution of these simulations. Unfortunately, and to the knowledge of the authors, there exist nowadays no other simulations for the last millennium that overcome this caveat. Thus, we use these two simulations that, although with limitations, have shown reasonable skill in similar contexts.

Although we compared in most cases outputs and results from both simulations, we mainly focus on ERIK2, since its initial conditions are probably a bit closer to real past variability (a bit colder than ERIK 1, see Gómez-Navarro et al. 2012). Output model daily data of temperature and precipitation are aggregated into seasonal values and standardized seasonal anomalies are built for each grid point and season (assessed with respect to mean values for the whole period 1001-1990). The ERIK1 simulation was continued from 1990 onwards under the SRES scenarios B2 and A2 (1990-2099) for the sake of producing two regional climate change projections, further described by Gómez-Navarro et al. (2010). These two scenarios correspond to two prominent scenarios included in the fourth IPCC report, that were reformulated for the sake of the fifth IPCC. As argued above, this choice is related to the time when these simulations were carried out, few years ago. Although these scenarios are somewhat outdated, the response of the modeled climate is consistent and based on physical relations that are independent on the definition of the scenario. Thus, the conclusions we draw regarding the co-variability of temperature and precipitation are not severely affected by the choice of scenario. Further, considering two different scenarios allows us to assess the uncertainty introduced by this choice.

First at all, temporal correlation coefficients between seasonal temperature (T) and precipitation (P) anomalies in each year are obtained for each grid point, for MM5-ERIK1 and MM5-ERIK2 simulations (1001-1990) and for future scenarios A2 and B2 (1990-2099) (run from the state of ERIK 1 in 1990). Assuming these raw interannual (seasonal) temperature and precipitation series to be non-autocorrelated, for the shorter future period (110 years), correlation coefficients reach the 5% significance level (t-test, p-value=0.05) for $|\rho|>0.19$. We mark the same level of correlation also for discussing correlation values for the paleosimulations in 1001-1990, in this case (990 years) corresponding to a p-value=0.001.

To analyze long-term variability in these correlation coefficients, we take 31 years moving windows to assess running correlation series between seasonal anomalies of temperature and precipitation. Seasons were considered as follows: winter, December to February (DJF); spring, March to May (MAM); summer, June to August (JJA); and autumn, September to November (SON). A regionalization exercise is performed using the correlation series at each grid point, for each season separately. In this way, we aim to identify regions with similar variability in seasonal precipitation-temperature relationship. The regionalization method is a k-means Cluster Analysis (CA), after applying a previous Principal Component Analysis (PCA) to filter noise in the data (Lorente-Plazas et al. 2014). The number of PCs retained is done following the next criteria: each one explaining more than 1% variability, and jointly all together explaining more than 90%. The CA is a two-step procedure. First, the choice of number of clusters for the k-means algorithm is based on a previous classification by means of the Ward algorithm (the tree-diagram enables to make a

choice of a number of well-separated classes in the data), which are used as seeds for the k-means. Moreover, a compromise is searched in order to retain a not very large number of clusters to make the analysis easier.

Once homogeneous regions are identified, we will make use of average regional series of temperature and precipitation anomalies, as well as regional P-T correlation series (assessed first at each grid point and thereafter averaged over the region), to characterize the co-variability patterns for all seasons in different regions of the IP. A wavelet transform analysis (Morlet wavelet) is performed to discover possible periodicities in the regional correlation series, which significance is tested by means of a REDFIT spectral analysis (Schulz and Mudelsee 2002, Allan et al. 2015).

Furthermore, we assess the modes of P-T covariability for each season and region as defined by López-Moreno et al. (2011): taking 40th and 60th percentiles of seasonal T and P, the modes are defined as: (1) cold/dry (CD; when T<T40 and P<P40); (2) cold/wet (CW; T<T40, P>P60); (3) warm/dry (WD; T>T60, P<P40); and (4) warm/wet (WW; T>T60, P>P60).

Subsequently, we check possible relationships of the regional series of correlation and the modes of covariability (both assessed in 31 years running windows) with the main variability modes of Sea Level Pressure (SLP) variability over the North Atlantic/European domain, extracted from ECHO-G global model (smoothed as well with 31 years moving windows). First of these modes resembles for all seasons the North Atlantic Oscillation pattern (NAO). Similarly, temporal linear correlations with anomalies of North Atlantic SST are also checked. We compute an Atlantic Multidecadal Oscillation index in the same way as assessed by Trenberth and Shea (2006): this is, we take average SST anomaly for the North Atlantic (0-60N), using a 70-year base period (1901–70) -as it covers roughly one full cycle of the AMO-. To deal with purely Atlantic variability, the global mean SST has been subtracted to derive the AMO index. Finally, composites maps are built to extract those circulation patterns (anomalies of SLP) linked to maximum and minimum correlation coefficients in the series. This may help in identifying physical mechanisms leading to strong/weak covariability.

3. Results and discussion

3. 1. Precipitation-temperature correlation maps (1001-1990)

Fig.1 shows mean correlation coefficients between seasonal temperature and precipitation series (anomalies in the period 1001-1990) considering ERIK2 simulation (similar values were obtained from ERIK1 simulation, presented together with projections in section 3.4). Contoured lines are drawn to mark significant values (at α=0.001) according to a 2-sides t-test (for sample N=990, ρ<-

0.19 and >0.19).

In winter (DJF) significant positive correlations arise for westernmost and central IP (mean correlation coefficients up to 0.54) (Fig. 1). This is meaningful since these regions are opened to the influence of warm and wet SW/W Atlantic flows, quite prevalent circulation in winter season (e.g., Fernández-Montes et al. 2012). Moreover, in winter, moisture availability in west IP and relatively cool atmospheric conditions enable a super C-C relationship (see Introduction). Hence it is natural that warm winters are concurrent with wet conditions in west Iberia (translating in positive correlation). Also, anomalous cold conditions in west IP in winter are usually driven by Atlantic subsidence and N/NE flow (Fernández-Montes et al. 2012) which provides moderate or under-normal precipitation totals (translating also to positive correlation). In contrast, significant negative correlations in winter appear for a wide area in the Mediterranean coast as well as Cantabrian coast and mountanious regions in eastern Iberian Peninsula (Fig. 1), where predominant W/SW circulation usually lead to warm and dry conditions, due to its location in rain-shadow areas (Fohën effect). Conversely, N/NE circulations and underlying cyclones are the most important configurations leading to significant precipitation in the Cantabrian/Mediterranean area (e.g., Fernández-Montes et al. 2012), those usually bringing cold air masses from higher latitudes. Therefore we can see how correlations in winter intensified when considering the interannual scale, with respect to low-frequency correlations maps (31 years running means of temperature and precipitation) assessed by Gómez-Navarro et al. (2012), where only the negative relationship for mountainous areas in northern and eastern IP arise (very limited positive signal in West IP).

In spring (Fig. 1), significant negative correlation coefficients (up to -0.61) are obtained for the whole of the Iberian Peninsula, highest absolute values appear towards mountainous areas to the north and the SE (the same regions with already negative or low correlations in winter season). It means that positive (negative) temperature anomalies usually relate to negative (positive) precipitation anomalies. For mountainous regions windward, a lift in the condensation level with temperature likely would explain an enhanced negative relationship (Lawrence 2005), as found in winter by Gómez-Navarro et al. (2012). Moreover, the spatial extent of correlation seems also to reflect, with respect to winter case, a greater importance of the precipitation-to-temperature causal relationship. This is, on one hand, cloudiness associated to cyclonic systems lead to less radiation and surface temperature, being the opposite true for stable anticyclonic conditions. And, on the other hand, negative precipitation anomalies in spring can give rise to a drying out of the soil, enhancing surface air temperature (enhanced sensible/latent heat ratio), having this feedback much more importance in summer than winter (Jerez et al. 2010; Jerez et al. 2012). This highly significant negative relationship in spring for the whole of the IP (as well as Northern Africa and Souhern France) is, to our knowledge, not previously reported in the literature.

In summer, also negative correlation coefficients arise (up to -0.64 to the NW), but only significant for the northern half of the Iberian Peninsula (W/NW, N and NE/E), i.e, for the regions with significant amount of precipitation as well as largest temperature and precipitation variability in summer season (Gómez-Navarro et al. 2011). In this warmest season, a negative causal relationship between precipitation and temperature anomalies seems logical, i.e., positive (negative) precipitation anomalies relates with negative (positive) temperature anomalies, explained via increased (decreased) cloudiness, wind/breezes and latent (sensible) heat fluxes (Berg et al. 2015).

Autumn P-T correlation pattern is a kind of "mixture" between winter and summer. Significant negative correlations for the whole period (1001-1990) appear only towards the NE and SE, especially in the Pyrenees, Iberian System, eastern Cantabrian coast and SE area (also mountanious regions). As argued for winter season, these regions are those more affected for N/NE cold and wet circulations. Moreover, mountanious regions (as in winter and spring) probably show an enhanced negative relationship due to a lift in the cloud condensation level with temperature (Lawrence 2005). In contrast, some positive correlations appear to the W and SW of the IP, but only significant for a small region to the SW: i.e., some positive Clausious-Clapeyron alike relationship (Berg et al. 2009) is observed for this region opened to warm and wet Atlantic air masses.

3.2. Regional series: changes in the covariability at different frequencies

Different regions are obtained for each season by applying k-means CA to the seasonal series of Pearson correlation coefficients between precipitation and temperature anomalies (31-years running windows). Initially, 804 grid point series are taken in the IP and part of Northern Africa. The results of this regionalization exercise are presented in Fig. 2. The frequency of covariability modes (cold-dry, cold-wet, warm-dry and warm-wet seasons) is assessed from regional series over the same 31-years running windows (see methods in section 2). Table 1 shows values of P-T correlation coefficients (at the interannual scale) and modes of covaribility (%) for each region, for the whole paelosimulation period 1001-1990.

For winter (DJF) season (Fig. 2a), 3 regions arise (first 3 PCs account for 94.8% of total variability); these regions are somehow easy to identify from Fig. 1. West and most central IP forms Region 1 (R1-win), with a correlation coefficient (over the whole period 1001-1990) between regional anomalies of temperature and precipitation of ρ= +0.43. This positive correlation is motivated by a larger frequency of warm-wet and cold-dry winters in this region (both with a mean frequency of 23%, see Table 1) with respect to warm-dry and cold-wet modes (~9%). Second cluster forms Region 2 (R2-win), comprising the Mediterranean coastal region, mountainous areas in eastern IP

(rain-shadow areas), part of Cantabrian coast (middle area), as well as the Pyrenees. Correlation coefficient for this region is ρ= -0.32. This is congruent with a larger mean frequency of warm-dry and cold-wet modes (20%) with respect to warm-wet and cold-dry modes (11%). Finally, Region 3 has a P-T correlation of ρ= +0.10 and comprises other mountainous areas in center and eastern IP (west of Region 2, i.e., more opened to Atlantic influence), as well as Ebro valley to the NE and parts of the Cantabrian region. Cold-dry and warm-wet modes are here only slightly more frequent than cold-wet and warm-dry winters. Corresponding regional correlation series (Fig. 2b) and covariability modes series (not shown) suffer large fluctuations over time. For example, for winter-Region 1, the 31-years correlation coefficient series take value from about 0 to near 0.6; for region 2, values go from -0.4 to 0. Moreover, these fluctuations are in phase between the 3 regions, i.e., correlation series of the 3 regions are highly correlated (especially R1 and R3 series, ρ=0.87). This seems to point to the influence of large-scale circulation variability in winter over the whole IP, which will be analyzed in next section.

For spring, 6 regions are identified: S/SE (R1), SW (R2), NE (R3), NW (R4), center-north IP (R4), and northern Africa (R6). Lowest negative correlation coefficients of the series are obtained towards north-center and eastern regions (around -0.5), meanwhile for western regions (R5 and R2) mean P-T correlation values are around -0.4. These western regions also depict the highest variability in the series. Nonetheless, all the 6 series oscillate around similar negatives values (contrary to the observed separation among regions in all the other 3 seasons, especially in winter). These negative coefficients in all the regions are motivated by much larger frequency of warm-dry (25%) and cold-wet modes (22%) with respect to cold-dry and warm-wet. Some of these regional series are also highly correlated, especially between neighbor regions: e.g., R1 with R2 (ρ=0.8), R2 with R5 (ρ= 0.77). In the low frequency, we can observe a period with minimum values (and less variance) around MCA (1100-1300), as well as in the last century. This seems to indicate a reinforcement of negative precipitation-temperature relationship in warmer periods.

For summer, 5 regions have been established. The regionalization and behavior of P-T correlation in summer is less clear, since precipitation in most IP is very low, and hence also anomalies are not very high (with respect to other seasons), giving rise to a difficult interpretation of the relationship. The lowest mean correlation coefficient in the series is that for R4 (comprising SE IP and some small northern Cantabrian areas), followed by R1 (NW and NE) (Table1). These are the regions with a largest frequency of warm-dry and cold-wet modes. However, it is likely that the origin of these modes is different, i.e., cold-wet summers in northern IP more related to intrusions of Atlantic cyclones, whereas the frequency of cold-wet modes in the SE can be more related with cloudiness and convective storms. Least strong correlations are those for R2 (south), where warm-wet mode is almost equally frequent than the warm-dry mode (probably due to larger frequency of storms in South Iberian Peninsula in warm summers, by the development of thermal low pressure)

and cold-dry mode is as frequent as cold-wet (less frequency of cold-wet compared to the North IP). These regional series also appear correlated among them for neighbor regions (e.g., ρ=0.79 between R2 and R3). In the low frequency, especially for R2 and R4, lowest values in the series are observed in mid-19th century onwards.

For autumn, also 5 regions are distinguished. Lowest values in these series are those for regions R5 (northern Africa), and R4 (coastal and mountainous regions in north/NE IP, ρ= -0.36), which are the regions with a largest frequency of warm-dry together with cold-wet modes. In agreement with correlation maps (Fig. 1), only SW region (R2) shows positive correlation values (+0.11 on average), related to a higher frequency of warm-wet and cold-dry autumns there, although less than in winter. In this case, and contrary to the rest of seasons, only R1 and R2 regional series (W/SW IP) show high temporal correlation (ρ=0.89) among them, being this below 0.45 for the rest of combinations of the regional series. This could point to a greater importance of local/regional effects in autumn season towards eastern and northernmost IP with respect to other seasons and regions.

We performed a wavelet transform analysis to the series of 31years running correlations in order to discover possible periodicities along the past millennium. For winter, peaks of periodicities appear in all the 3 series at a frequency of about 49-51 years (see supplementary material, Fig. S2), detected by means of a REDFIT spectral analysis (Schulz and Mudelsee 2002). This peak in the power spectrum of the time series is significantly different (at 99% level) from a red-noise spectrum for all the 3 winter regions. In spring, for R5 (NW IP), R4 (N-centre), and R1 (SE), significant peaks in the spectrum above the false-alarm levels is also detected around 63-64 years (Supplementary material, Fig. S2). Moreover, for the case of R5-spring (NW IP), another highly significant peak is found at 94-95 years (power spectrum above 1.4). In Fig. 5 we show the results for the wavelet transform of this regional correlation series, jointly to the plot of temperature and precipitation anomalies evolution for this region. Highest squared correlation strength (power) can be detected for periods >60 years, while noise remains for lower periods. In this Fig. 3. 3 we also see how periods of lowest correlation (about -0.4/-0.5) are concurrent with highly negative precipitation and positive temperature anomalies. For summer, no significant periodicities are detected, although highest power also appears for periods >60 years. These periodicities in the correlation coefficient -especially found here for spring season- are in line with that found for the NW Alps (reconstructed P-T series for the last millennium) in the extended warm season (May to August) by Amann et al. (2015). They suggested a possible modulation of the AMO in this P-T relationship. For autumn, only in R5 series (Northern Argelia) a significant periodicity of about 87 years is found (Fig. S2), which might relates to AMO variability (Knudsen et al. 2011). In the next section we will explore the possible fingerprint of atmospheric circulation patterns and Atlantic SST in the P-T covariability modes.

3.3. Physical mechanisms

To check if main atmospheric and/or oceanic variability modes are affecting the series of correlation, as well as the covariability modes (CD, CW, WD, WW) we extract from our simulation (from the global ECHO-G model) North Atlantic Sea Level Pressure (SLP) and Sea Surface Temperature (SST) modes of variability (see methods section 3). In the case of SLP, first EOF resembles closely NAO pattern for all seasons, whereas second EOF is closed to the East Atlantic (EA) pattern, especially for spring (the Atlantic low pressure centre is displaced further east in the case of winter and autumn EOF2). For Atlantic SST, a first mode of variability, resembling the Atlantic Multidecadal Oscillation (AMO) is used (Fig. S3, see Methods). Correlations were higher when considering the frequency of covarialitiy modes (Table 2) than for running correlation series (not shown), likely due to the fact that the same correlation values can be related to very different atmospheric conditions (e.g., positive correlations in winter due to either cold-dry or warm-wet modes). Therefore, in Table 2, we show temporal Pearson correlation coefficients between these atmospheric and oceanic modes of variability (applying 31 years running means) and the series of frequency of covariability modes (in 31 years running windows). Because of space constraints and to analyze and highlight main relationships, we have tabulated only those combinations of regions/modes giving rise to some correlation values above 0.3 (bold values). Significant correlation values at the 95% confidence level are assessed according to a bootstrap method (Ebisuzaki, 1997), taking into account the 31-years filters of the series (marked with *, $|\rho|>0.38$), as in Gómez-Navarro et al. (2012).

The AMO index shows largest fingerprint in spring and summer, with negative/positive correlation coefficients with the frequency of cold/warm modes (Table 2). However, the 95% confidence level is only reached with the cold-dry mode for spring-R6 (Northern Africa and SE corner of the IP), with $\rho= -0.54$ and with the warm-wet mode for spring-R1 (Central/SE/E of the IP), with $\rho= +0.39$. Correlations between AMO and the series of running correlations take values up to -0.29 for summer-R2 and spring-R6 (not shown). By contrast, in winter and autumn, the relationship with the AMO is much weaker. This means that, for summer and spring, positive (negative) phases of the AMO are significantly related to positive (negative) air surface temperature anomalies, being as well the negative P-T correlation enhanced under AMO+. This points to a greater influence of large-scale Atlantic SST variability patterns on spring and summer temperature anomalies -as well as on the link with precipitation-, and may therefore indicate a modulation of the AMO on the P-T covariability in these seasons. Hence, this might well in part explain the periodicity signal of about 60-65 years found in spring correlation series (Fig. 5). This relationship of the AMO with covariability modes could be due to a significant influence of Atlantic SST –in phase or one month in advance, and mainly from the tropical band- on North Atlantic atmospheric circulation in spring,

found both in observations and models (Frankignoul et al. 2003) (in the model the influence extent until late summer), involving changes in the Hadley circulation and in the NAO and ENSO patterns. Moreover, the North Atlantic (NA) SST horseshoe anomaly pattern (largely related with the AMO) has been recently found to be in part generated by spring and summer atmospheric variability, also detected both models and observations during the last 500 years (Gastineau et al. 2013). This important (and mostly in-phase) ocean-atmosphere coupling in spring and summer can therefore explain a larger influence of the AMO on the P-T covariability in these seasons.

The NAO pattern depicts linear correlations with the frequency of cold-wet (negative) and warm-dry (positive) modes in winter, spring and autumn, especially for western regions (Table 2). These results are in agreement with López-Moreno et al. (2011) who found, for IP mountains in 1950-2006, winters with warm-dry (cold-wet and warm-wet) conditions linked to highest (lowest) NAO values, meanwhile cold-dry winters were associated with intermediate NAO values. Also the cold-wet mode for R1-winter is related to the EA pattern (EOF2, ρ= -0.34), in congruence with observational studies for the NW IP (Lorenzo et al. 2008). However, the cold-wet mode is not the most frequent one in winter (but the warm-wet and cold-dry modes, see Table 1); these prevalent modes inducing positive correlations in R1-winter are not significantly correlated with main modes of SLP variability.

In spring, a high correlation (ρ= -0.43) is obtained between NAO and the frequency of warm-dry mode in Region 5 (W/NW IP), which is the most frequent P-T mode (Table 1), linked with a negative P-T correlation. Therefore, these results seem to indicate that both NAO and AMO have somehow been acting simultaneously over spring covariability series, given that both patterns depict indeed a periodicity of about 60-70 years (Higuchi et al. 1999; Knudsen et al. 2011). Moreover, as mentioned above, AMO (Atlantic SST) and NA atmospheric circulation in spring depict a significant interrelation both at interannual (Frankignoul et al. 2003) and decadal timescales (Gastineau et al. 2013).

In autumn, the second mode of variability depicts a significant correlation with the frequency of cold-dry modes for R1 (central-NW-south IP ρ= -0.42) (Table 2), which is meaningful given the underlying cold and dry NE advection in its negative phase (anticyclone in West Europe). Although non significantly, this pattern also relates with the frequency of cold-wet modes in autumn in the SE/E region (R3), likely due to the formation of back-door cold fronts with easterly cold advection over the warm Mediterranean Sea in autumn (Fernández-Montes et al. 2014). Moreover, the pattern in its positive phase relates with the frequency of warm-wet modes for most IP (ρ= 0.37 for R1-au), which is also meaningful given the advection of moisture air from the Atlantic Ocean.

Checking all these relationship (Table 2, Table 1) we find out that, with the exception of spring,

(when warm-dry/cold-wet modes appear related to NAO+/NAO-), the most frequent modes of P-T covariability for each region and season do not appear significantly correlated to main SLP modes of variability. Thus, to get a deeper insight into the physical mechanisms leading to maximum and minimum values of correlation in the regional series, we assess composite patterns of SLP over the European-north Atlantic domain corresponding to periods with correlation above 90th and below 10th percentile, for each region and season. SLP model simulations (from ECHO-G) were available for the period 1501-1990.

Fig. 4 shows results for winter (DJF) season. Composites maps of SLP anomalies corresponding to those 31-years periods in which P-T correlations are below/above the $10^{th}/90^{th}$ percentile of the series are plotted for each region. Approximately 45 winters are averaged in each composite pattern. We see that maximum correlation values in all the 3 regions are related to low pressure anomalies intensified in the Mediterranean region (right panel), with a gradient to slightly positive SLP anomalies northwest of the IP, enhancing N/NE circulation over the IP. Then it is natural that these patterns are related to negative temperature anomalies in all the 3 regions (larger for R3, with average Tanomalies= - 0.3) and near to 0 precipitation anomalies. The composite patterns corresponding to 31-years periods with correlation bellow 10th percentile (left panel) are somehow opposite: especially for R2 and R3, positive pressure anomalies appear in the Mediterranean and central-north Europe. In all the three regions, average temperature and precipitation anomalies are near 0 for these patterns. It means that it is very likely that several configurations with different T/P anomalies (leading to similar values of correlations) have been averaged.

Therefore, we did sub-composites of SLP maps within these patterns corresponding to temperature above/bellow $70^{th}/30^{th}$ percentiles (of temperature distributions in the 45 seasons previously average). These T percentiles were taken in order to retain a considerable number of cases (~13/14 winters in each pattern). In Fig. 4b these results are shown for winter Region 1 (corTP>90th percentile = +0.6) and Region 2 (for corTP <10th percentile= -0.32). In the case of R1 (west-central IP) the sub-composites for T<T30^{th} (= -0.70) shows similar but "more extreme" pattern, i.e., larger SLP gradient between the low in the Mediterranean/Central-east Europe and a high pressure anomaly west of British Island, thus showing an intensified N cold and dry advection. Mean R1 precipitation anomalies for this pattern (14 winters averaged) is -0.81. On the contrary, the sub-composite map for T>T70^{th} (= 0.27) shows low pressure anomalies in the Atlantic west of the IP (positive anomalies north almost disappeared) at the same time than a slightly more western location of Mediterranean low pressure anomaly. This configuration produces average precipitation anomalies for R1 of +0.81. Therefore, we see how relatively small shifts in the intensity and position of SLP anomalies centers can give rise to very different (opposite) temperature and precipitation anomalies in winter, both configurations related to very high values (ρ>0.6) of correlation. For R2 and lowest negative correlation values, sub-composites also

provides very opposite patterns: while for T>T70[th] (= 0.42) positive SLP anomalies are centered over the Mediterranean enhancing subsidence and thus producing below normal precipitation (mean precipitation anomalies = -0.55), for T<T30[th] (= -0.56) the high pressure anomaly is intensified over the north-west and central Europe, together with a relative negative anomaly SW of the IP, producing above normal precipitation anomalies (+0.58). Therefore, we conclude that all these patterns corresponding to maximum and minimum P-T correlations in winter are related to enhanced N/NE and S/SE (meridional) circulations rather than to changes in zonal circulation.

For spring SLP, composite maps corresponding to periods with maximum negative correlation values (i.e., |ρ|< 10th percentile ~ -0.53) are related for most regions to positive SLP anomalies over the Atlantic NW of the IP (i.e., probably linked with enhanced to NAO+), on average leading to above normal temperature and slightly negative precipitation anomalies (not shown). As an exception, Reg 5(NW) pattern for intense negative correlation show a low pressure anomaly in the Atlantic (related to NAO-) providing average colder and wetter than normal conditions. This is congruent with the significant correlations between P-T covariability modes and NAO found in spring (Table 2). However, T and P anomalies associated to these patterns are weak, since composite maps are hiding patterns related to both very positive and negative anomalies of the variables, especially for lowest correlation patterns (not shown), as in the winter case (Fig. 4b). Autumn composites patterns are, for some regions (mainly R4- NE IP, which is the region depicting highest negative correlation- see Table 1, Fig. 2), somehow related to the winter case, i.e., maximum absolutes values in correlations (not very strong in autumn) related to enhanced NE to SE circulations (not shown). Contrary to winter and spring, for summer and autumn most negative correlations values are usually obtained under relatively cold and –for summer- wetter than normal conditions, but in these seasons composites patterns are less clear and more region-dependent, suggesting again a larger influence of local factors (e.g., convective precipitation, clouds, and other regional feedbacks) in autumn and summer with respect to larger large-scale atmospheric influence in winter and spring. Sub-composites patterns for these regions were not further analyzed.

3.4. Regional projections in the P-T covariability

Fig. 5 shows results for ERIK 1 simulation and future scenarios B2 and A2 (1990-2099, run from the state of ERIK1 in 1990). The same correlation level as in Fig. 1, |ρ|>0.19, is taken in the contour plot (alpha=0.05 for future projections, alpha=0.001 for ERIK1 paleo-simulation). First than all, we see that spatial patterns of correlation coefficients between seasonal temperature and precipitation for ERIK1 (Fig. 5, left panel) are very similar to those obtained for ERIK2 (Fig.1). Basically, only for summer season and for some mountainous regions in southeastern IP, areas

with significant negative correlations in ERIK1 are slightly narrowed than those in ERIK2 simulations.

Important changes in correlation patterns for future scenarios B2 and A2 (1991-2099) can be observed with respect to ERIK1 (Fig. 5, middle and right panels). For winter, the significant positive correlations in west and central IP almost disappear in B2 projections (confined to small areas in A2 scenario), while negative correlations move southwards, being enhanced towards the SE IP (especially mountainous regions) in both scenarios. This seems to indicate a change in P-T relationship in future scenarios, having winters more similar to past autumn conditions (Fig. 5, map of SON, ERIK1). This is likely due to a translation towards warmer conditions (Gómez-Navarro et al. 2010). Moreover, this is congruent with an increase in the mean magnitude of the NAO simulated by global models for future decades (López-Moreno et al. 2011), which implies larger frequency of warm-dry modes with respect to cold-wet modes..

In spring, negative values of correlations –significant in the whole IP- are also reinforced (Fig. 5) in both scenarios, with the exception of small areas in the Ebro and Guadalquivir valleys. Apart from the possible effect of changes in circulation patterns like the NAO, the warming itself projected in future scenarios (Gómez-Navarro et al. 2010) is likely acting towards and enhanced negative relationship, i.e, via intensification of the positive soil moisture-atmosphere feedback, as it has been highlighted for summer (Jerez et al. 2010; Jerez et al. 2012).

For summer season, future significant negative correlations are less spread than in the paleosimulation and are confined to northernmost and NW IP. Nonetheless, over mountainous regions in SE IP this negative relationship is enhanced (as in winter), likely related to an increase in the condensation level with temperature (Lawrence 2005). Moreover, some positive signals appear in the SW of the IP (Guadalquivir valley), which could indicate an inversion in P-T relationship in this area due to more intense convective precipitation with increasing temperature (e.g., Berg et al. 2009). Indeed, according to previous simulations for the IP, summer convective precipitation is projected to increase due to further intensification of the convective rainfall -rather than to an increase in the number of this kind of event- (Jerez et al. 2012). However, it is also likely that the loss of significant negative relationship (and inversion towards slightly positive correlations) is motivated by the fact that precipitation and precipitation variability is very small in summer, and specially in this southern region, and then negative precipitation anomalies reach a minimum very soon in future scenarios.

In autumn, the difference among the two scenarios (Fig. 5) is the largest: For B2 scenario, the spatial extension of negative correlation values is reduced to the Pyrenees and mountains to the SE, i.e., the highest mountains in the IP, where a lift in the condensation level with temperature

explains the negative link (as in the other seasons). In the rest of the IP, the non-significant P-T correlation might be motivated by enhanced convective precipitation with increasing temperature (and SST), i.e., a positive relationship counteracting the negative link. However, in a more emissive A2 scenario (warmer projections, see Gómez-Navarro et al. 2010), significant P-T negative correlation is obtained in most IP, especially towards mountainous regions North and East, with the exception of the Mediterranean coast and coastal NW and SW regions. This is, only regions affected by moisture maritime air masses (where higher frequency and intensity of precipitation is common in autumn), remains without a negative P-T relationship. In this case, it is likely that enhanced warming lead to a lift in the condensation level in most central IP (although especially in the mountains). .

4. Conclusions

Regional climate paleosimulations (1001-1990) for the Iberian Peninsula (IP) have been used to analyze the joint variability of seasonal anomalies of temperature (T) and precipitation (P). On the one hand, the use of high-resolution regional climate models (MM5, 30 km) has enabled to discover important regional relationships –due to the complex orography and climate regimes of the IP- which have not been detected in the previous literature analyzing P-T covariability, given the use of courser resolution data (global observations or models, see Introduction). On the other hand, the separation among seasons (winter, spring, summer, autumn) has also enabled to detect inter-seasonal signals not reported before, since published studies had traditionally focused mainly in winter and summer, not considering the transition seasons separately. Thus, previous works analyzing P-T anomalies on interannual timescales had principally found negative (slightly positive) correlations for summer (winter) for the majority of IP (e.g., Trenberth and Shea 2005), without any regional detail. One the most significant features that arises from the present work is a highly significant negative P-T relationship in spring for the whole of the IP. Moreover, this negative correlation is found strongest and stands as well for the rest of seasons for mountainous regions towards the north, east, and SE IP, given a predominance of warm-dry together with cold-wet modes. By contrast, in western regions in winter a significant positive P-T relationship is found, this signal was not apparent analyzing P-T correlations on longer timescales (i.e., after applying 31-years smoothing P and T series) (Gómez-Navarro et al. 2012).

Furthermore, the length of the data (millennium-long) has made possible to check the variability of P-T relationships and the frequency of the covariability modes (cold-wet, cold-dry, warm-wet, warm-dry) over a long period. Different regions in the IP were defined for each season according to the evolution of seasonal P-T correlation (assessed in 31-years moving windows). The analysis reveals strong decadal to multidecadal variability in all regions and seasons. In summer and autumn the separation among regions in mean values and variability is strongest, suggesting an

important role of local radiative processes (i.e., convective rainfall, clouds, etc…) in these seasons.

In winter, the variability of the regional correlation series is highly coherent among the 3 main regions identified (although separated in mean values, positive towards west-central and negative towards eastern and northern IP, and around 0 for an intermediate region). Significant periodicities of about 50 years are found in all these 3 winter regional series. The fingerprint of the North Atlantic Oscillation (NAO) is significant over the frequency of cold-wet (negative) and warm-dry (positive) modes, being these two the less (most) frequent modes in winter (spring) in west-central IP. Thus, it is found out that the highest correlation values in winter are related with enhanced meridional (N/NE or S/SE) or easterly circulation, as it is also found for autumn in some regions. In spring, most regions (especially western) depict very high multidecadal variability in the P-T correlation series, arising significant periodicities of about 60-65 years (also at 95 years for NW region), detected by means of wavelet transform analysis. In this spring season, the fingerprint of the NAO is obvious in all regions, being significantly related with the frequency of the most frequent covariability modes (i.e., cold-wet and warm-dry). Moreover, both in summer and, especially, in spring, the Atlantic Multidecadal Oscillation (AMO) also depicts significant relationship with the frequency of cold (negative) and warm (positive) modes, hence likely explaining in part the significant periodicities in the P-T correlation series.

Future work is required to better characterize the physical mechanisms explaining changes in the P-T covariability at interannual and longer time scales, e.g., the way in which oceanic and atmospheric variability relate to each other and affect the covariability (as for spring) in the different regions. Furthermore, the analysis of the P-T covariability on shorter timescales is also desirable, i.e, by considering model daily data of P and T (e.g, Berg et al. 2009). Another further improving in the understanding of P-T relationships would come from the separation between large scale and convective precipitation (Jerez et al. 2012). Finally, even for shorter time periods and on a local scale, the comparison of these results with available climatic data from paleo-reconstructions (e.g., documentary data, Rodrigo et al. 2012) would help in identifying possible similarities/divergences, and may improve the confidence on the relationships found here from MM5 model simulations.

References

Adler RF, Gu G, Wang JJ, Huffman GJ, Curtis S, Bolvin D. (2008). Relationships between global precipitation and surface temperature on interannual and longer timescales (1979-2006). J. Geophys. Res. 113: D22104, doi: 10.1029/2008JD010536.

Amann, B., Szidat, S., & Grosjean, M. (2015). A millennial-long record of warm season precipitation and flood frequency for the North-western Alps inferred from varved lake sediments: implications for the future. Quaternary Science Reviews, 115, 89-100.

Berg, P., J. O. Haerter, P. Thejll, C. Piani, S. Hagemann, and J. H. Christensen (2009), Seasonal characteristics of relationship between daily precipitation intensity and surface temperature, J. Geophys. Res., 114, D18102, doi:10.1029/2009JD012008.

Berg, A., Lintner, B. R., Findell, K., Seneviratne, S. I., van den Hurk, B., Ducharne, A., ... & Gentine, P. (2015). Interannual Coupling between Summertime Surface Temperature and Precipitation over Land: Processes and Implications for Climate Change. Journal of Climate, 28(3), 1308-1328.

De Luis M, Brunetti M, Gonzalez-Hidalgo JC, Longares LA, Martin-Vide J. (2010). Changes in seasonal precipitation in the Iberian Peninsula during 1946-2005. Global and Planetary Change 74: 27-33

Déry, S. J., and E. F. Wood, (2005): Observed twentieth century land surface air temperature and precipitation covariability, Geophys. Res. Lett., 32, L21414, doi:10.1029/2005GL024234.

Ebisuzaki, W. (1997): A method to estimate the statistical significance of a correlation when the data are serially correlated, Journal of Climate, 10, 2147–2153, 1997.

Estrella N, Menzel A. (2013). Recent and future climate extremes rising from changes to the bivariate distribution of temperature and precipitation in Bavaria, Germany. Int. J. Climatol. 33:1687–1695.

Fernández-Montes S, Seubert S, Rodrigo FS, Hertig E (2012). Wintertime circulation types over the Iberian Peninsula: long-term variability and relationships with weather extremes. Clim Res 53: 205−227

Fernández-Montes S, Seubert S, Rodrigo FS, Rasilla Alvarez DF, Hertig, E, Esteban P, Philipp A. (2014). Circulation types and extreme precipitation days in the Iberian Peninsula in the transitions seasons: spatial links and temporal changes. Atmos. Res. 138: 41–58.

Frankignoul, C., Friederichs, P., & Kestenare, E. (2003). Influence of Atlantic SST anomalies on the atmospheric circulation in the Atlantic-European sector. Annals of Geophysics.

Gastineau, G., D'Andrea, F., & Frankignoul, C. (2013). Atmospheric response to the North Atlantic Ocean variability on seasonal to decadal time scales. Climate dynamics, 40(9-10), 2311-2330.

Gómez-Navarro, J. J., Montávez, J. P., Jiménez-Guerrero, P., Jerez, S., Garcia-Valero, J. A., and González-Rouco, J. F. (2010): Warming patterns in regional climate change projections over the Iberian Peninsula, Meteorol. Z., 19, 275–285, 2010.

Gómez-Navarro, J. J., Montávez, J. P., Jerez, S., Jiménez-Guerrero, P., Lorente-Plazas, R., González-Rouco, J. F., and Zorita, E. (2011): A regional climate simulation over the Iberian Peninsula for the last millennium, Clim. Past, 7, 451–472, doi:10.5194/cp-7-451-2011.

Gómez-Navarro, J.J., Montávez, J. P., Jiménez-Guerrero, P., Jerez, S., Lorente-Plazas, R., González-Rouco, J.F., and Zorita, E. (2012): Internal and external variability in regional

simulations of the Iberian Peninsula climate over the last millennium, Clim. Past, 8, 25–36, doi:10.5194/cp-8-25-2012.

Gomez-Navarro, J.J.; Zorita, E. (2013): Atmospheric annular modes in simulations over the past millennium: No long-term response to external forcing. Geophysical Research Letters DOI: 10.1002/grl.50628

Higuchi K, Huang J, Shabbar A. (1999). A wavelet characterization of the North Atlantic Oscillation variation and its relationship to the North Atlantic sea surface temperature. International Journal of Climatolology, 19: 1119 – 1130.

Jerez, S., Montavez, J.P., Gomez-Navarro, J.J., Jimenez-Guerrero, P., Jimenez, J., Gonzalez-Rouco, J.F. (2010). Temperature sensitivity to the land-surface model in MM5 climate simulations over the Iberian Peninsula. Meteorol.Z. 19 (4), 363–374.

Jerez, S.,Montavez, J.P., Gomez-Navarro, J.J., Jimenez, P.A., Jimenez-Guerrero, P., Lorente, R., Gonzalez-Rouco, J.F. (2012). The role of the land-surface model for climate change projections over the Iberian Peninsula. J. Geophys. Res. 117, D01109. http://dx.doi.org/10.1029/2011JD016576.

Knudsen, M.F., Seidenkrantz, M.-S., Jacobsen, B.H., Kuijpers, A., (2011). Tracking the Atlantic multidecadal oscillation through the last 8,000 years. Nat. Commun. 2, 178.

Lawrence MG. (2005). The relationship between relative humidity and the dewpoint temperature in most air: a simple conversion and applications. Bull. Am. Met. Soc. 86: 225-233.

Li, G. Q., S. P. Harrison, P. J. Bartlein, K. Izumi, and I. C. Prentice, (2013): Precipitation scaling with temperature in warm and cold climates: An analysis of CMIP5 simulations. Geophys. Res. Lett.,40, 4018–4024, doi: 10.1002/grl.50730.

López-Moreno JI, Vicente-Serrano SM, Morán-Tejeda E, Lorenzo-Lacruz J, Kenawy A, Beniston M (2011) Effects of the North Atlantic Oscillation (NAO) on combined temperature and precipitation winter modes in the Mediterranean mountains: observed relationships and projections for the 21st century. Global Planet Change 77:62−76

Lorente-Plazas R, Montavez JP, Jimenez PA, Jerez S, Gomez-Navarro JJ, García-Valero P, Jimenez-Guerrero JA. (2014). Characterization of the surface wind over the Iberian Peninsula. Int. J. Climatol., doi:10.1002/joc.4034

Lorenzo,M.N., Taboada, J.J., Gimeno, L., (2008). Links between circulation weather types and teleconnection patterns and their influence on precipitation patterns in Galicia (NW Spain). Int. J. Climatol. 28, 1493–1505.

Rebetez, M., (1996): Seasonal relationship between temperature, precipitation and snow cover in a mountainous region. Theor. Appl. Climatol., 54(3–4), 99–106.

Rodrigo, F. S., Gómez-Navarro, J. J., & Montávez Gómez, J. P. (2012). Climate variability in Andalusia (southern Spain) during the period 1701–1850 based on documentary sources: evaluation and comparison with climate model simulations. Climate of the Past, 8(1), 117-133.

Rodrigo, F. S. (2014). On the covariability of seasonal temperature and precipitation in Spain, 1956–2005. International Journal of Climatology. DOI: 10.1002/joc.4214

Schulz, M., Mudelsee, M., (2002). REDFIT: estimating red-noise spectra directly from unevenly spaced paleoclimatic time series. Computers and Geosciences 28, 421-426.

Schurer A.P., Tett S.F.B. and Hegerl G.C. (2013). Small influence of solar variability on climate

over the past millennium. Nature Geoscience. DOI: 10.1038/NGEO2040

Tout, D. G., (1987): Precipitation-temperature relationship in England and Wales summers. Int. J. Climatol.,7(2), 181–184.

Trenberth K E and Shea D J (2005). Relationships between precipitation and surface temperature Geophys. Res. Lett. 32 L14703

Trenberth, K.E., and Shea DJ (2006), Atlantic hurricanes and natural variability in 2005, Geophys. Res. Lett., 33, L12704, doi:10.1029/2006GL026894.

Trenberth KE. (2011). Changes in precipitation with climate change. Clim. Res. 47: 123–138

Wu, R. G., J. P. Chen, and Z. P. Wen, (2013): Precipitation–surface temperature relationship in the IPCC CMIP5 Models. Adv. Atmos. Sci., **30**(3), 766–778, doi: 10.1007/s00376-012-2130-8.

Table1. Pearson correlation coefficients between regional seasonal temperature and precipitation anomalies (P-T correlation, * indicates significant linear correlations at p-value<0.001) for the whole paleosimulation 1001-1990, (first column) as well as mean frequency of the co-variability modes (cold-dry, cold-wet, warm-dry, and warm-wet) in the same period (next four columns, in bold most frequent modes), for each region and season.

Winter (DJF)	P-T correlation	Cold-Dry (%)	Cold-Wet (%)	Warm-Dry (%)	Warm-Wet (%)
R1-win	**0,43***	**22,9**	9,0	9,1	**23,2**
R2-win	**-0,32***	11,5	**20,1**	**20,7**	11,2
R3-win	0,10	**17,5**	15,1	14,1	**17,7**
Spring (MAM)					
R1-sp	**-0,50***	9,4	20,7	**25,8**	10,8
R2-sp	**-0,40***	6,8	20,4	**24,8**	12,5
R3-sp	**-0,51***	9,1	21,1	**27,4**	6,4
R4-sp	**-0,53***	7,8	23,9	**26,4**	9,6
R5-sp	**-0,42***	8,7	20,5	**26,6**	10,4
R6-sp	**-0,42***	5,2	**23,3**	**23,2**	13,5
Summer (JJA)					
R1-su	**-0,51***	8,1	**26,7**	22,9	7,3
R2-su	**-0,33***	10,9	**21,6**	**19,4**	11,6
R3-su	-0,09	**16,1**	**16,9**	15,8	**15,0**
R4-su	**-0,59***	6,6	**25,5**	**25,1**	6,2
R5-su	**-0,27***	10,9	**20,3**	**21,1**	11,3
Autumn (SON)					
R1-au	-0,01	**15,5**	**16,6**	15,2	**16,0**
R2-au	0,11	**17,1**	14,0	14,2	**17,8**
R3-au	**-0,19***	12,8	**19,5**	**18,9**	13,5
R4-au	**-0,36***	10,2	**22,4**	**20,7**	10,0
R5-au	**-0,37***	9,7	**23,1**	**22,2**	9,6

Table 2. Pearson correlations coefficients between the modes of covariability (frequency in 31 years running windows) and the concurrent Atlantic Multidecadal Oscillation (AMO, 31 years running means of Atlantic SST anomalies), North Atlantic Oscillation (EOF1 of SLP anomalies over NA/Europe), and second EOF2 of SLP (both 31 years running means). Only those covariability modes and regions with correlation coefficients above 0.3 in at least one case are included in the table. (CD= cold-dry, CW= cold-wet, WD= warm-dry, and WW= warm-wet, *correlation significant at p-value<0.05)

|	Winter (DJF)	AMO	NAO(EOF1)	EOF2
CW	R1-win	-0,14	**-0,49***	**-0,34**
	R3-win	-0,17	**-0,40***	-0,26
WD	R1-win	0,19	**0,38***	0,08
	Spring (MAM)	**AMO**	**NAO (EOF1*-1)**	**EOF2**
CD	R6-sp	**-0,54***	-0,20	0,09
CW	R1-sp	-0,07	**-0,35**	-0,09
	R2-sp	-0,16	**-0,38***	0,15
	R3-sp	**-0,35**	-0,29	0,01
	R4-sp	-0,09	**-0,33**	0,09
WD	R2-sp	**0,30**	**0,34**	-0,08
	R3-sp	0,24	**0,37**	-0,19
	R4-sp	0,15	**0,31**	-0,06
	R5-sp	0,27	**0,43***	-0,12
	R6-sp	0,14	**0,30**	0,09
WW	R1-sp	**0,39***	0,12	-0,08
	R2-sp	**0,30**	0,05	0,08
	Summer (JJA)	**AMO**	**NAO (EOF1*-1)**	**EOF2*-1**
CD	R1-su	**-0,35**	-0,11	0,12
	R2-su	**-0,31**	-0,12	-0,02
WD	R2-su	**0,31**	0,27	-0,12
WW	R2-su	-0,12	0,19	**0,31**
	R3-su	-0,06	**0,36**	0,19
	Autumn (SON)	**AMO**	**NAO (EOF1*-1)**	**EOF2**
CD	R1-au	0,05	-0,20	**-0,42***
CW	R1-au	-0,09	**-0,32**	-0,08
	R3-au	-0,16	-0,18	**-0,33**
	R5-au	-0,13	-0,16	**-0,34**
WD	R1-au	0,10	**0,33**	-0,02
	R2-au	0,06	**0,38***	-0,10
	R4-au	0,10	**0,34**	0,11
	R5-au	0,14	0,20	**0,35**
WW	R1-au	0,12	0,02	**0,37**
	R3-au	-0,04	0,12	**0,30**
	R4-au	0,25	0,24	**0,33**
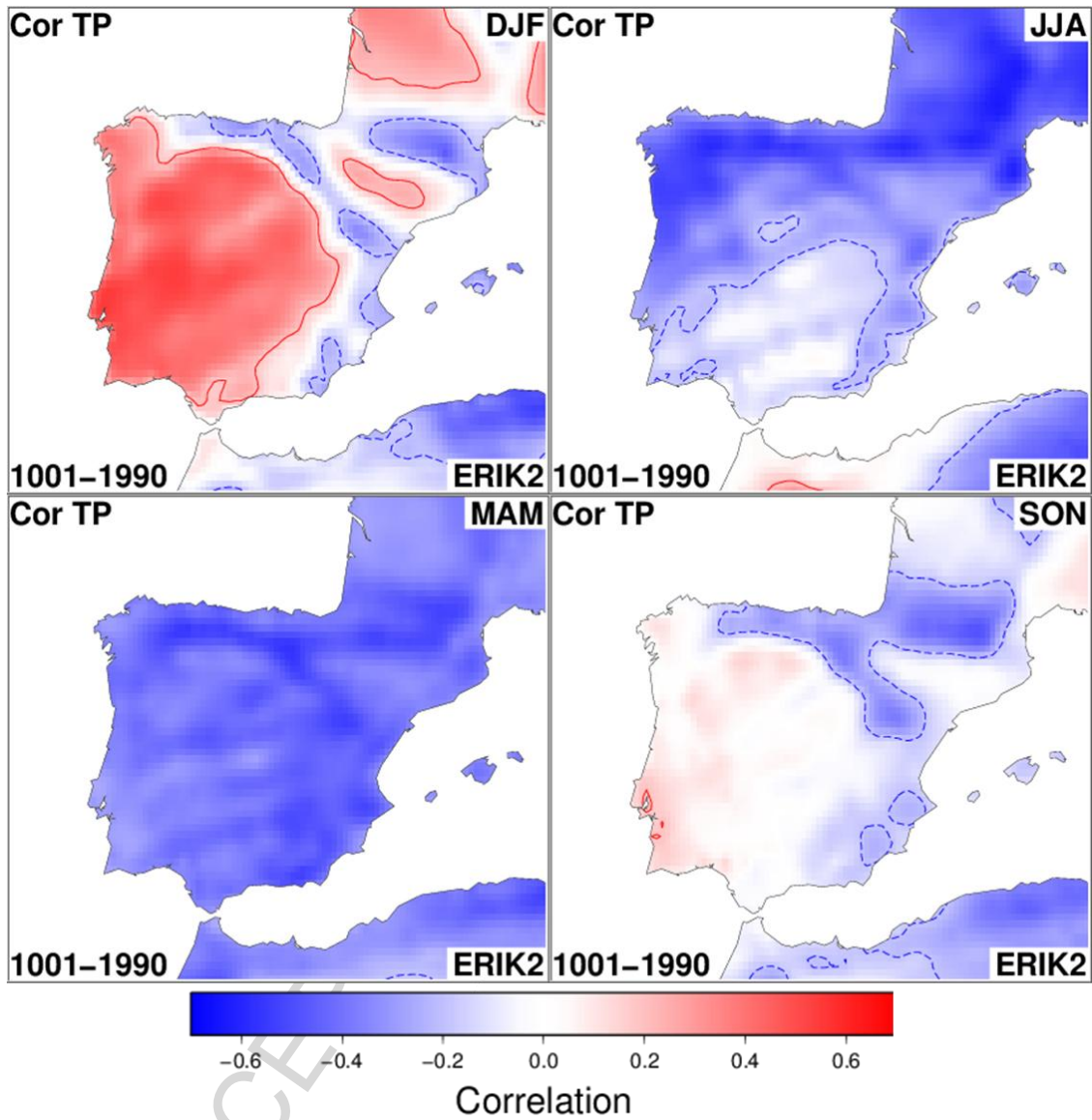
Fig. 1. Pearson linear correlation coefficients (ρ) between seasonal anomalies of temperature and precipitation in 1001-1990 (ERIK2 ECHO-G-MM5 paleosimulation). Contour lines delimit values significant at p-value=0.001 (|ρ|>0.19).
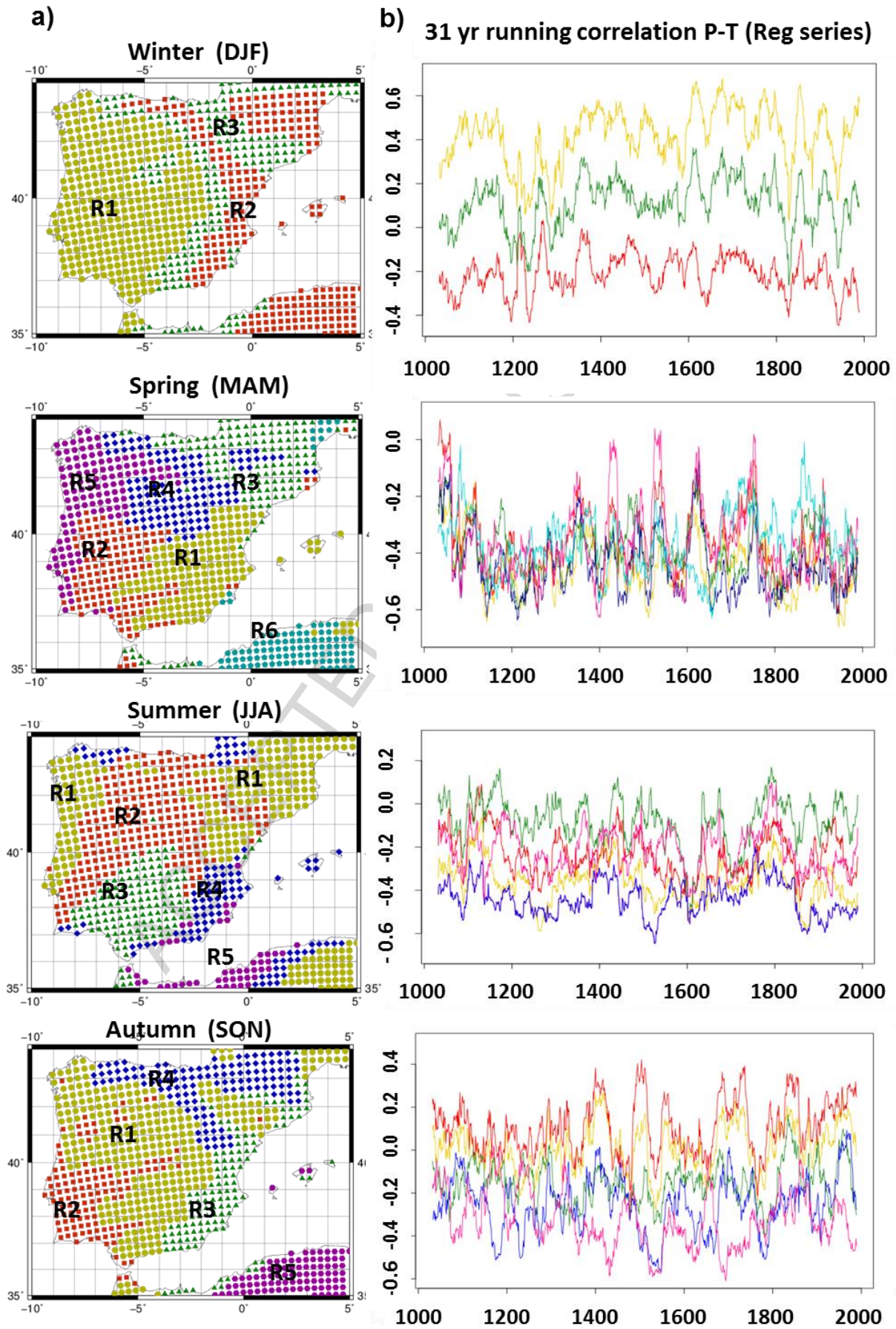
a)

b)

Fig. 2. Regions and corresponding precipitation-temperature (P-T) correlation coefficient regional series (obtained between seasonal T and P anomalies in 31 years running windows) for MM5-ERIK2 simulation.
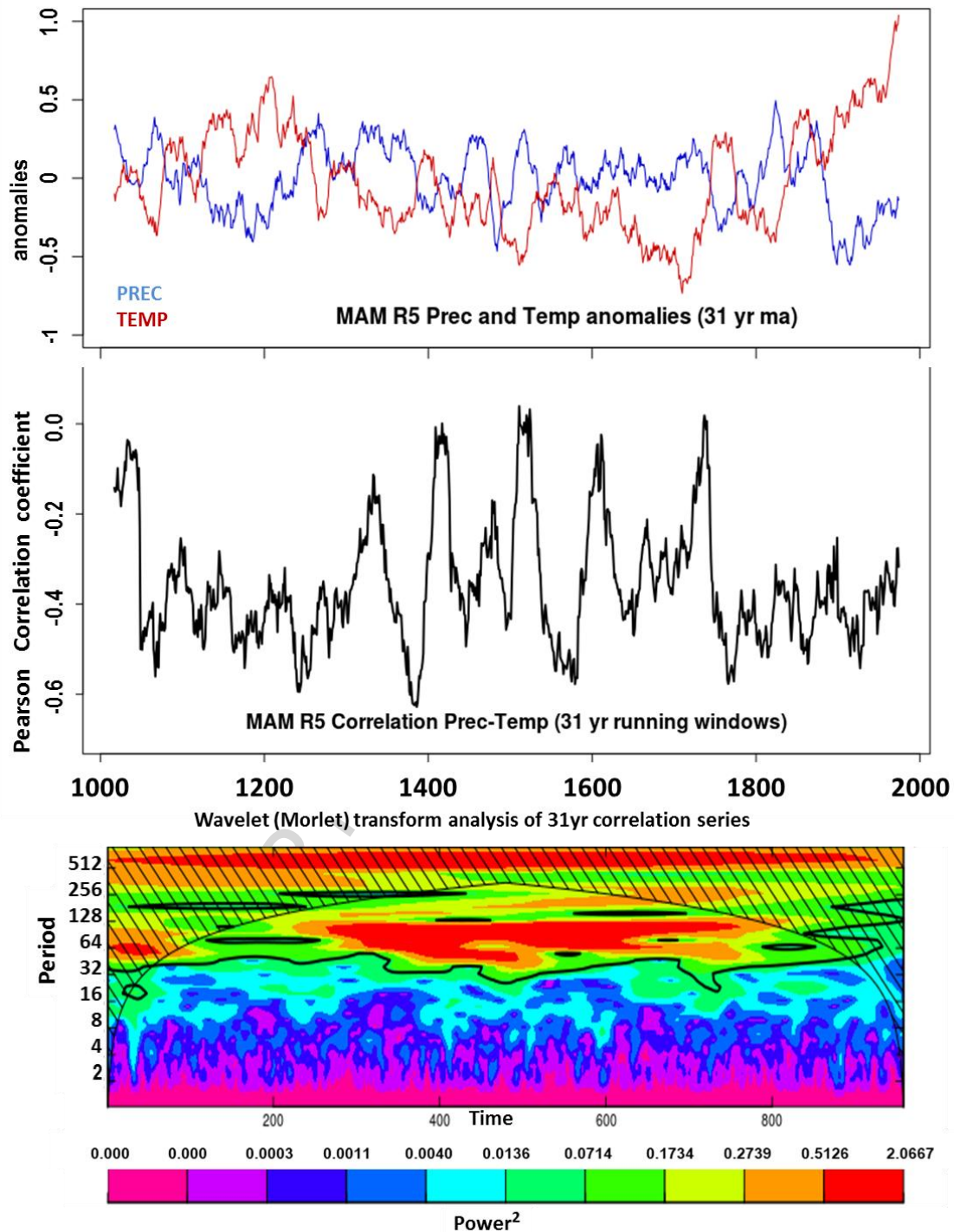
Fig. 3. Wavelet transform of regional P-T correlation series for R5-spring. Highest squared correlation strength (power) can be detected for periods >50-60 years, while noise remains for higher frequencies (shorter periods). Similarly, temperature and precipitation series (smoothed by 31 years filters) for this R5-spring region are plotted above.
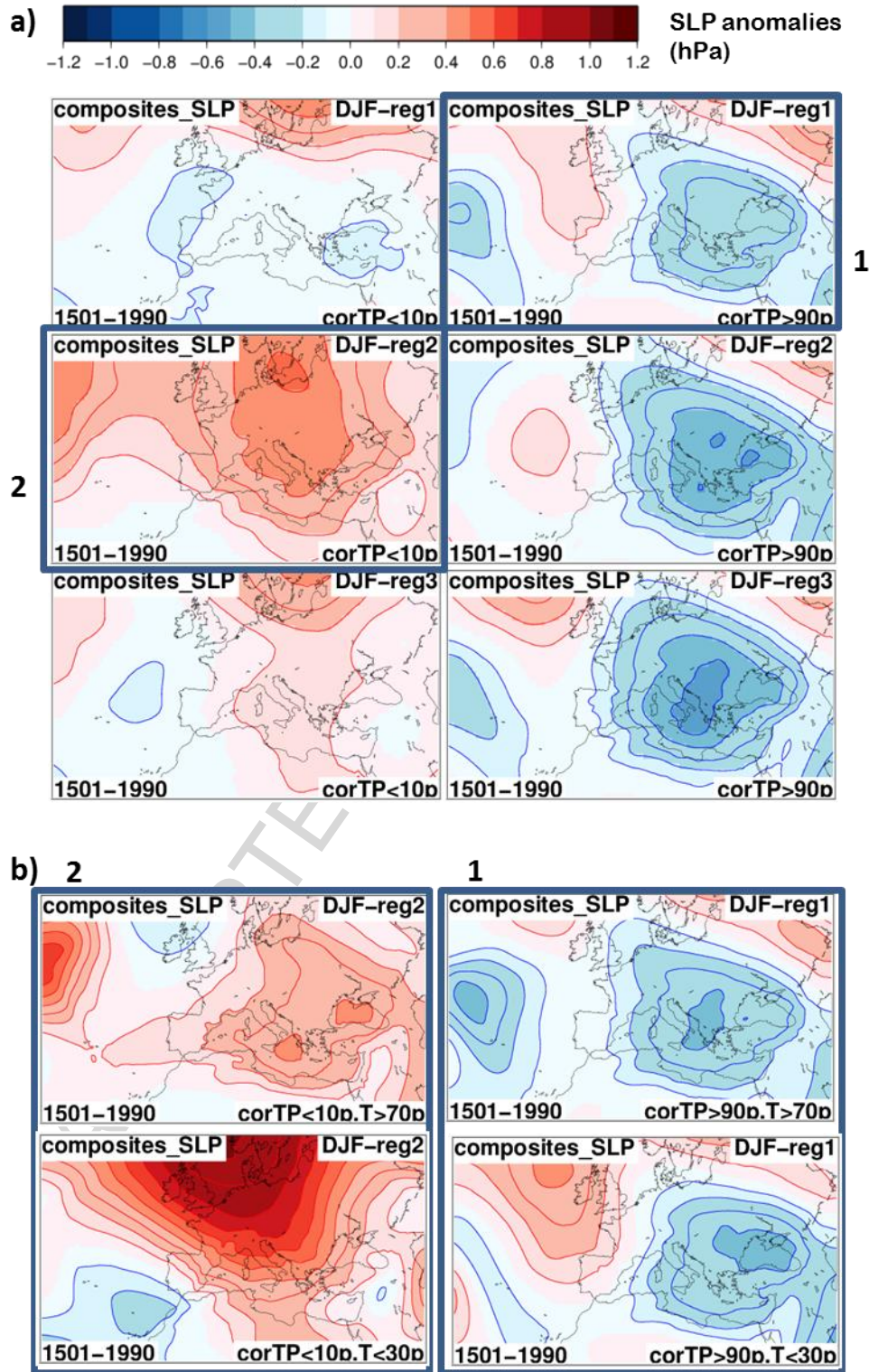
Fig. 4 a) Composites of SLP for maximum and minimum values P-T correlation coefficients (SLP is extracted from the 31years windows in which correlation is above or bellow 90/10 percentiles). b) Sub-composites of 2 of the previous SLP patterns (1 and 2) for temperature above and below 70th / 30th percentiles.
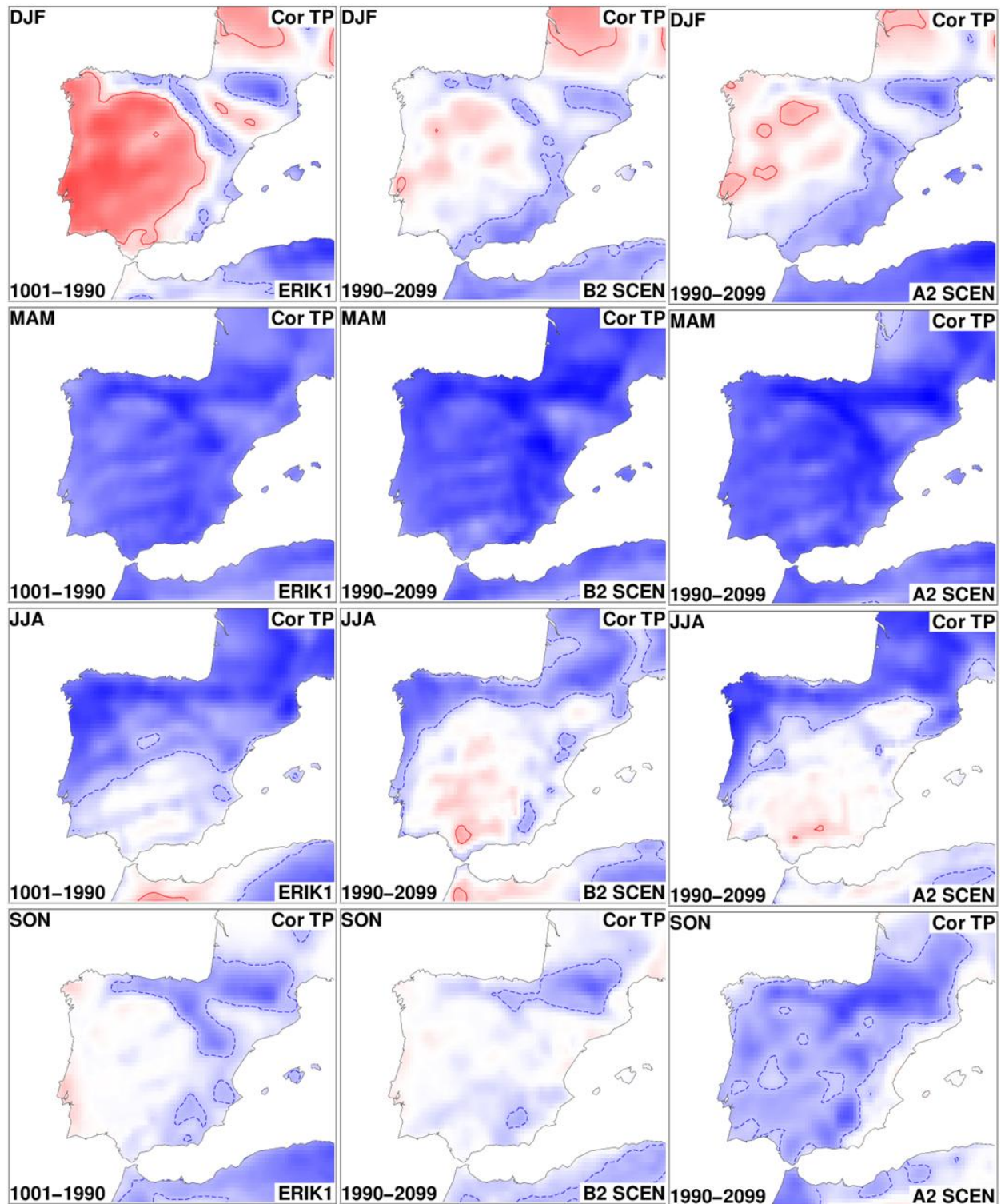
Fig. 5. Temporal Pearson correlation coefficients (ρ) between seasonal temperature and precipitation anomalies in each year (interannual covariability) for a) the paleosimulation ERIK1 and b) Future simulations under SRES scenarios B2 and c) A2. Dashed lines delimit regions with correlation coefficient above 0.19 (red) and bellow -0.19 (blue), linked with p-value=0.05 for projections in the 110 year period 1990-2099 (p-value=0.001 for the paleosimulation ERIK1 in 1001-1990).

Highlights:

Regional simulations for the Iberian Peninsula are employed (1001-2099)

Precipitation-temperature relationship is studied.

Positive correlations dominate west-central region in winter.

Negative correlations arise in mountainous regions in all seasons.

In spring, all regions depict negative correlations, enhanced in warmer periods.